PERGAMON

International Journal of Solids and Structures 40 (2003) 4519–4548

INTERNATIONAL JOURNAL OF SOLIDS and STRUCTURES

www.elsevier.com/locate/ijsolstr

Thermomechanical constitutive equations for the dynamic response of ceramics

E. Bar-on [a,*], M.B. Rubin [b], D.Z. Yankelevsky [c]

[a] *Rafael Ballistics Center (24), P.O. Box 2250, Haifa 31021, Israel*
[b] *Faculty of Mechanical Engineering, Technion-Israel Institute of Technology, Haifa 32000, Israel*
[c] *Faculty of Civil Engineering, Technion-Israel Institute of Technology, Haifa 32000, Israel*

Received 8 July 2002

Abstract

The behavior and failure of brittle materials is significantly influenced by the existence of inhomogeneities such as pores and cracks. The proposed constitutive equations model the coupled micro-mechanical response of these inhomogeneities through evolution equations for scalar measures of porosity, and a "density" function of randomly oriented penny-shaped cracks. A specific form for the Helmholtz free energy is proposed which incorporates the known Mie–Grüneisen constitutive equation for the nonporous solid. The resulting thermomechanical constitutive equations are valid for large deformations and the elastic response is hyperelastic in the sense that the stress is related to a derivative of the Helmholtz free energy. These equations allow for the simulation of the following physical phenomena exhibited by brittle materials: (1) high compressive strength compared with much lower tensile strength; (2) inelastic deformation due to growth and nucleation of cracks and pores instead of due to dislocation dynamics associated with metal plasticity; and (3) loss of integrity (degradation of elastic moduli) due to damage accumulation. The main features of the model are demonstrated by examples of cyclic loading in homogeneous deformation and by a simulation of a dynamic plate-impact experiment on AD85 ceramic. The theoretical predictions of the model are in excellent agreement with the dynamic experimental data.

Keywords: Constitutive equations; Porosity; Fracture; Brittle; Ceramics; Dynamic

1. Introduction

A major cause for the failure of ceramics is brittleness due to the existence of micro-structural cavities such as pores and cracks. These cavities usually appear in many shapes, and in sizes that range from crystal size (nuclei boundaries) up to tens of microns. Since the number and type of these cavities in a real material is so large, it is impossible to analyze the evolution of each one individually. Consequently, it is necessary to use

* Corresponding author. Tel.: +972-4879-2459; fax: +972-4879-2113.
E-mail address: ebaron@rafael.co.il (E. Bar-on).

0020-7683/03/$ - see front matter © 2003 Elsevier Ltd. All rights reserved.
doi:10.1016/S0020-7683(03)00211-7

Nomenclature

$\bar{a}$	average radius of a penny-shaped crack in the present configuration
$\bar{a}_0$	average radius of a penny-shaped crack in the reference configuration
a	radius of a penny-shaped crack in the present configuration
A	material constant that controls the decrease in the yield stress due to pore collapse
A_{C}^1	history-dependent function that depends on stress (open cracks)
A_{C}^2	history-dependent function that depends on stress (closed cracks)
$\tilde{\mathbf{A}}$	symmetric tensor that characterizes the relaxation effects of plasticity on the evolution of elastic distortional deformation
B	material constant in the exponent of the function that decreases the yield stress due to pore collapse
b_{s}^t	a function that controls the deviation of porosity during dilation from the porosity associated with zero pressure, when the crack damage effect is included
b_0^t	material constant controlling the deviation of porosity during dilation from the porosity associated with zero pressure when no crack damage is included
$\mathbf{B}_{\mathrm{e}}'$	elastic distortional deformation tensor
C_v	specific heat of the solid
C_1, C_2, C_3	material constants controlling porosity rate
C_{R}	Rayleigh wave speed of the material
$\mathrm{d}v$	element of total volume in the present configuration
$\mathrm{d}v_{\mathrm{p}}$	element of pore volume in the present configuration
$\mathrm{d}v_{\mathrm{s}}$	element of solid volume in the present configuration
$\mathrm{d}V$	element of total volume in the reference configuration
$\mathrm{d}V_{\mathrm{p}}$	element of pore volume in the reference configuration
$\mathrm{d}V_{\mathrm{s}}$	element of solid volume in the reference configuration
D_{C}	a generalized measure of crack damage
D_{u}	uniaxial deformation rate
$\mathbf{D}$	rate of deformation tensor, symmetric part of $\mathbf{L}$
$\mathbf{e}_i$	rectangular Cartesian base vectors
E_{zz}	total Lagrangian axial strain
f	function that controls compaction rate
f_1, f_2	functions defining the Helmholtz free energy
f_3	function that controls compaction rate
f_{C}	material parameter that characterizes the friction coefficient between crack surfaces
$\mathbf{F} = \partial\mathbf{x}/\partial\mathbf{X}$	the total deformation gradient
$F_{\mathrm{s}}(\theta)$	the value of the relative volume of the solid associated with zero pressure
g	yield function
$\mathbf{g}$	temperature gradient
G_{i}	instantaneous strain energy release rate
G_{C}	critical strain energy release rate
G_{I}	strain energy release rate due to MODE I
G_{II}	strain energy release rate due to MODE II
G_{STATIC}	acting strain energy release rate
$H(x)$	Heavyside function
$\mathbf{I}$	second order unity tensor

I	a variable that describes material integrity
J	total relative volume
J_u	total relative volume in the unloaded state
J_s	relative volume of the solid
K_{IC}	static fracture toughness
$\mathbf{L}$	velocity gradient
n	number of cracks per unit reference volume
$\hat{n}_b$	evolution function for the nucleation of cracks due to the branching phenomenon
$\hat{n}_C$	evolution function for the nucleation of cracks due to pore crushing
$\mathbf{n}$	a unit vector perpendicular to crack plane
n	number of cracks per unit volume in the present configuration
n_0	number of cracks per unit volume in the reference configuration
p	total pressure
p_s^c	pressure in the fractured solid
p_s	pressure in the intact solid
p_{s1}	part of the pressure in the solid associated with dilatation and temperature
p_s'	part of the pressure in the solid mainly due to elastic distortional deformation
p_{sH}	pressure on the Hugoniot
p_{crush}	value of the pressure at the onset of porous compaction
p_d	function controlling the magnitude of the pressure during porous dilation
$\mathbf{p}$	entropy flux vector per unit present area
$\mathbf{q}$	external rate of heat flux per unit present area
r	specific external rate of heat supply
s	specific external rate of supply of entropy
S_1, S_2, S_3	material constants that specify the shock velocity versus particle velocity curve
t	time
$\mathbf{T}$	Cauchy stress tensor
T_{ij}	Cauchy stress tensor's components
$\mathbf{T}'$	deviatoric part of the Cauchy stress
$\mathbf{T}_s'$	deviatoric part of the Cauchy stress in the solid
U_s	shock-wave velocity
$\mathbf{v}$	velocity of a material point
$\mathbf{x}$	position vector of a material point in the present configuration
$\mathbf{X}$	position vector of a material point in the reference configuration
Y	yield strength in uniaxial stress
Y_0	reference value of the yield strength
$\langle x \rangle$	Macauley brackets
α_1	invariant of elastic distortional deformation
γ_s	Grüneisen gamma for the solid in the present configuration
γ_0	Grüneisen gamma for the solid in the reference configuration
Γ	function controlling the magnitude of elastic distortional deformation
ε	specific internal energy
ε_{s1}	part of the specific internal energy of the solid associated with dilatation and temperature
ε_s'	part of the specific internal energy of the solid mainly due to elastic distortional deformation
ε_{sH}	specific internal energy on the Hugoniot
$\hat{\mu}_s$	shear modulus function

μ_0	shear modulus of the intact solid in the reference configuration
η	specific entropy
η_s	specific entropy of the solid
η_s^c	specific entropy of the fractured solid
η_{s1}	specific entropy of the solid associated with dilatation and temperature
η_s'	specific entropy of the solid mainly due to elastic distortional deformation
α, β	spherical polar angles
θ	absolute temperature
θ_0	value of the absolute temperature θ in the reference configuration
ν	Poisson's ratio
ξ	specific internal rate of production of entropy
ξ'	specific internal rate of entropy production due to material dissipation
ξ_d'	specific internal rate of entropy production due to inelastic distortional deformation
ξ_ϕ'	specific internal rate of entropy production due to porosity changes
ξ_C'	specific internal rate of entropy production due to crack damage
ξ_1, ξ_2	auxiliary variables
κ_1, κ_2	dimensionless material parameters controlling crack growth rates
κ_3, κ_4, κ_5	dimensionless material parameters controlling crack nucleation rates
ρ	mass per unit present total volume
ρ_0	mass per unit reference total volume
ρ_s	mass of the solid per unit present solid volume
ρ_{s0}	mass of the solid per unit reference solid volume
σ_e	Von Mises effective stress
σ_N	the normal stress acting on a crack's plane
σ_T	the tangential stress acting on a crack's plane
Φ	porosity in the reference configuration
ϕ	porosity in the present configuration
ϕ_s	dilation porosity function
ϕ_u	unloaded porosity in the present configuration
ϕ_u^0	unloaded porosity in the reference configuration
ϕ_u^{min}	minimum value of unloaded porosity attained during loading
ψ	specific Helmholtz free energy
ψ_C	specific surface energy due to the formation of cracks
ψ_s	specific Helmholtz free energy of the solid
ζ_C	specific crack "density", a measure for crack damage

some averaging procedure or simplifying modeling assumptions to predict the response of macroscopic structures.

During the last 50 years there has been considerable success using linear elastic fracture mechanics to characterize the effective properties of materials containing idealized flaws. Kachanov et al. (1994) summarize much of this work and present expressions for effective moduli of materials with many interacting cavities.

An alternative approach is to use notions of continuum damage mechanics (Krajcinovic, 1996) which generalize the early work of Kachanov (1958) for rupture under creep conditions. In this approach, it is common to introduce damage parameters (scalars or tensors) which characterize the reduction in elastic

moduli and which are determined by integrating phenomenological evolution equations. Within this context, an attempt is made to predict the evolution of the damaged state.

The objective of this paper is to develop thermomechanical constitutive equations, which model the response of ceramics to dynamic shock loading. Due to the nonlinear-coupled thermomechanical nature of shock loading it is essential to model measurable Hugoniot data. Also, due to the micro-cracking that occurs in ceramics it is desirable to incorporate known results of fracture mechanics into the constitutive equations. This paper attempts to blend phenomenological modeling in macroscopic nonlinear continuum mechanics with known results of fracture mechanics to motivate more micro-mechanically based phenomenological evolution equations for various internal state variables that characterize the failure process.

To this end, the concept of a representative volume element (RVE) is used; Hill (1963), Hashin (1964, 1983), Kröner (1977), Willis (1981), and Nemat-Nasser (1986). As stated by Nemat-Nasser and Hori (1993, p. 11), "An RVE for a material point of a continuum mass is a material volume which is statistically representative of the infinitesimal material neighborhood of that material point. The continuum material point is called a *macro-element*. The corresponding micro-constituents of the RVE are called the *micro-elements*. An RVE must include a very large number of micro-elements, and be statistically representative of the local continuum properties". More specifically, the material is considered to be a composite material composed of a solid matrix and cavities. The cavities are modeled by uniformly distributed spherical pores and penny-shaped cracks, with the cracks being randomly oriented.

Kachanov (1994) has commented on difficulties combining fracture mechanics and phenomenological continuum damage mechanics. One such difficulty (pointed out by Ju, 1990) occurs when a single damage parameter is used to reduce the strain energy function. This assumption causes Poisson's ratio to remain unaffected by damage, which is inconsistent with results from fracture mechanics. Within the present context, the effects of damage evolution on the dilatational response and on the distortional response (deviatoric stress) are modeled independently. Moreover, since the constitutive equations are hyperelatic (with the stress being determined by a derivative of the Helmholtz free energy) and since damage depends on the stress state due to friction on the crack faces, special care must be taken to ensure that the second law of thermodynamics is properly satisfied. This is accomplished by introducing four history-dependent variables: the unloaded porosity ϕ_u (related to the current porosity ϕ, Eq. (45)) to model the dilatational response; the average crack radius $\bar{a}$ (Eq. (19a)), the number of cracks per unit reference volume n (Eq. (22)), and a damage parameter D_C (Eq. (29)) associated with cracking, which modifies the shear modulus. All four variables are determined by integrating time-dependent evolution equations. Also, the evolution equation for D_C incorporates friction and depends on an integral over all possible fracture orientations. Moreover, these evolution equations are based on a Maxwell–Boltzmann distribution function for crack lengths.

The resulting constitutive equations incorporate the Mie–Grüneisen equation of state for the nonporous solid and they allow for the simulation of the following physical phenomena exhibited by brittle materials:

1. High compressive strength compared with much lower tensile strength.
2. Inelastic deformation due to growth and nucleation of cracks and pores instead of due to dislocation dynamics associated with metal plasticity.
3. Loss of integrity (degradation of elastic moduli) due to damage accumulation.

These model features were examined using a computer code which determines the material response of a single RVE to specified homogeneous deformations. Also, the model was implemented into a two-dimensional axi-symmetric Lagrangian shock-wave code, and a simulation of a plate-impact experiment on AD-85 ceramic was performed. The resulting theoretical predictions of the model are in excellent agreement with the dynamic experimental data.

The structure of this paper is as follows: Section 2 briefly describes the thermomechanical equations used to develop the constitutive model. Section 3 motivates the functional forms of the phenomenological

evolution equations for fracture, based on micro-mechanical equations for penny-shaped cracks. Section 4 discusses the equations for porous compaction and dilation, Section 5 presents the constitutive equations for the intact matrix and Section 6 presents the constitutive equations for the cracked, porous material. Section 7 presents a number of examples to examine the range of material response predicted by the model. In particular, it is shown that the model can produce excellent agreement with dynamic plate-impact experiments. Also, Section 7 includes simulations which exhibit the sensitivities to various model parameters which can be used to help determine the values of these constants that best simulate a specific experiment. Finally, Section 8 presents a brief summary of the results.

2. Thermomechanical background

Let $\mathbf{X}$ denote the location of a material point in the fixed-reference configuration and $\mathbf{x}$ denote the location of the same material point in the deformed present configuration at time t. Also, let $\mathbf{F} = \partial\mathbf{x}/\partial\mathbf{X}$ be the deformation gradient and $\mathbf{C} = \mathbf{F}^{\mathrm{T}}\mathbf{F}$ be the right Cauchy–Green total deformation tensor. Following the thermodynamic procedures proposed by Green and Naghdi (1977, 1978), the local form of the balance of entropy can be written as

$$\rho\dot{\eta} = \rho(s + \xi) - \operatorname{div}\mathbf{p}, \tag{1}$$

where ρ is the density (mass per unit volume), η is the specific (per unit mass) entropy, s is the specific external rate of supply of entropy, ξ is the specific rate of internal production of entropy, and $\mathbf{p}$ is the entropy flux vector per unit present area. A superposed dot denotes material time differentiation holding $\mathbf{X}$ fixed, and div denotes the divergence operator with respect to the present position $\mathbf{x}$. Furthermore, the quantities s and $\mathbf{p}$ are related to the specific rate of heat supply r and the heat flux $\mathbf{q}$ per unit present area (appearing in the balance of energy) by the expressions

$$s = \frac{r}{\theta}, \quad \mathbf{p} = \frac{\mathbf{q}}{\theta}. \tag{2a, b}$$

In general, ξ can be separated into two parts (Rubin, 1992)

$$\rho\theta\xi = -\mathbf{p}\cdot\mathbf{g} + \rho\theta\xi', \tag{3}$$

where $\mathbf{g} = \partial\theta/\partial\mathbf{x}$ is the temperature gradient with respect to the present configuration, and $\mathbf{p}\cdot\mathbf{g}$ denotes the usual scalar product between two vectors. Thus, Eqs. (1)–(3) can be used to obtain

$$\rho r - \operatorname{div}\mathbf{q} = \rho\theta\dot{\eta} - \rho\theta\xi'. \tag{4}$$

Also, it is recalled that with the help of the conservation of mass and the balance of linear momentum, the balance of energy can be written in the form

$$\rho\dot{\varepsilon} = \rho r - \operatorname{div}\mathbf{q} + \mathbf{T}\cdot\mathbf{D}. \tag{5}$$

In this equation, ε is the specific internal energy, $\mathbf{T}$ is the Cauchy stress, $\mathbf{D}$ is the symmetric part of the velocity gradient $\mathbf{L}$, such that

$$\mathbf{v} = \dot{\mathbf{x}}, \quad \mathbf{L} = \partial\mathbf{v}/\partial\mathbf{x}, \quad \mathbf{D} = \frac{1}{2}(\mathbf{L} + \mathbf{L}^{\mathrm{T}}), \tag{6}$$

where $\mathbf{A}\cdot\mathbf{B} = \operatorname{tr}(\mathbf{A}\mathbf{B}^{\mathrm{T}})$ is the inner product between two second order tensors $\mathbf{A}$ and $\mathbf{B}$, and the balance of angular momentum has been used to impose the restriction that $\mathbf{T}$ is symmetric.

In their work, Green and Naghdi (1977, 1978) developed restrictions on constitutive equations by requiring the balances of angular momentum and energy to be satisfied for all thermomechanical processes. Specifically, by using (4) and the definition

$$\psi = \varepsilon - \theta\eta, \tag{7}$$

for the specific Helmholtz free energy (HFE), the balance of energy (5) can be rewritten in the reduced form

$$\rho(\dot{\psi} + \eta\dot{\theta}) - \mathbf{T}\cdot\mathbf{D} + \rho\theta\xi' = 0. \tag{8}$$

Furthermore, these constitutive equations are required to satisfy statements of the second law of thermodynamics, which include the condition that heat flows from hot to cold

$$-\mathbf{p}\cdot\mathbf{g} > 0 \quad \text{for } \mathbf{g} \neq 0 \tag{9}$$

and the condition that the material dissipation is nonnegative (Rubin, 1992)

$$\rho\theta\xi' \geqslant 0. \tag{10}$$

3. Fracture mechanics

It is assumed that the brittle material is a homogenized continuum with a sufficient number of penny-shaped cracks that they can be dealt with statistically. More specifically, the cracks are distributed homogeneously and randomly so that the crack size distribution function is independent of the specific locations or orientations of the cracks. One such distribution has been described in detail by Bar-on and Yankelevsky (1993) and is called the Maxwell–Boltzmann distribution function for crack lengths

$$w_a(n,\bar{a},a) = \frac{32na^2}{\pi^2\bar{a}^3}\exp\left[-\frac{4}{\pi}\left(\frac{a}{\bar{a}}\right)^2\right], \tag{11a}$$

where

$$n = \int_0^\infty w_a(n,\bar{a},a)\,\mathrm{d}a \quad \text{and} \quad \bar{a} = \frac{1}{n}\int_0^\infty w_a(n,\bar{a},a)a\,\mathrm{d}a, \tag{11b,c}$$

are the number of cracks per unit reference volume, and the average crack radius, respectively, and a is the crack radius. The parameters n and $\bar{a}$ are calculated by integrating evolution equations that will be derived in the following sections.

This distribution function is used to determine the integrated influence of all cracks in the RVE on the material response to any arbitrary loading. In this model, it is assumed that this distribution function is valid even when n and $\bar{a}$ change. Also, since the cracks are assumed to have random orientations, mutual effects cancel (Kachanov, 1992), so crack interactions are ignored.

3.1. Criterion for crack growth and nucleation

In fracture mechanics the strain energy release rate G (rate here refers to crack extension and not to "time"), or alternatively, the crack driving force, was introduced by Griffith (1924), such that

$$G = \frac{\mathrm{d}}{\mathrm{d}a}(W - U), \tag{12}$$

where W is the strain energy in the body due to external work, and U is the surface energy due to crack generation.

The value of G at any instant is denoted by G_i and its critical value, associated with crack extension, is denoted G_C

$$G_C = \frac{K_{IC}^2(1-v)}{2\mu_0}, \tag{13}$$

where the fracture toughness K_{IC} is a temperature-dependent material parameter, taken in this work to be constant, μ_0 is the shear modulus in the reference configuration and v is the reference value of Poisson's ratio.

Expressions for the instantaneous energy release-rate for MODE I and for MODE II, have been proposed by Keer (1966) and Rice (1984), respectively. These papers deal with a single crack under static or quasi-static loading, whereas, in this work the instantaneous energy release rate associated with dynamic response is computed in a RVE subjected to the current stress-state at each time-step. In addition, here the contribution of all cracks in the element is determined using the crack distribution function.

To this end, it is convenient to introduce the normal stress σ_N and shear stress σ_T applied to the crack's surface

$$\sigma_N = \mathbf{n}\cdot\mathbf{Tn}, \quad \sigma_T = \sqrt{|\mathbf{Tn}|^2 - \sigma_N^2}, \tag{14a, b}$$

where $\mathbf{n}$ is a unit vector normal to this surface.

For the case of a single crack loaded statically, the energy release rate G_i is computed by the following expressions:

1. For a tensile stress $\sigma_N \geqslant 0$ acting normal to the crack's surface, the value of G is given by (Eq. (27) in Keer (1966))
$$G_I = \frac{2(1-v)}{\pi\mu_0} a\left[\sigma_N^2 + \frac{2}{2-v}\sigma_T^2\right]. \tag{15a}$$
2. For a compressive stress $\sigma_N < 0$ acting normal to the crack's surface, the value of G is given by (Eq. (9) in Rice (1984))
$$G_{II} = \frac{4(1-v)}{\pi\mu_0(2-v)} a\langle\sigma_T + f_C\sigma_N\rangle^2, \tag{15b}$$
where f_C is a material parameter characterizing the friction coefficient between the crack's surfaces, and the Macauley brackets are defined by
$$\langle x\rangle = \tfrac{1}{2}(|x| + x). \tag{16}$$

Using these expressions, the instantaneous energy release rate G_i in the RVE is calculated by weighting the static value with the crack density distribution function $w_a(n, \bar{a}, a)$, such that

$$G_i = \frac{1}{2\pi n}\int_0^{2\pi}\int_0^{\pi/2}\int_0^{\infty} w_a(n,\bar{a},a) G_{STATIC}\, da \sin\alpha\, d\alpha\, d\beta, \tag{17}$$

where α and β are spherical polar angles and

$$G_{STATIC} = \left\{\begin{array}{ll} G_I & \text{for } \sigma_N \geqslant 0 \\ G_{II} & \text{for } \sigma_N < 0 \end{array}\right\}. \tag{18}$$

3.2. Crack growth and nucleation

3.2.1. Crack growth

The expression for crack growth used here is a modification of the expression given by Rajendran et al. (1989, 1990). Specifically, the evolution law for the average crack length $\bar{a}$, is determined by a strain energy release rate criterion of the form of

$$\dot{\tilde{a}} = \kappa_1 C_R \left\langle 1 - \left(\frac{G_C}{G_i} \right)^{\kappa_2} \right\rangle, \quad C_R = \frac{0.862 + 1.14\nu}{1 + \nu} \sqrt{\frac{\mu}{\rho}}, \tag{19a, b}$$

where C_R is the Rayleigh wave speed (Eq. (5.100) in Achenbach (1973)) and κ_1, κ_2 are dimensionless material parameters that are determined by calibrating simulations of impact experiments. Notice that the crack length will not increase until the Griffith criterion $[G_i > G_C]$ is satisfied. Moreover, the shear stress σ_T influences the response for both tensile and compressive normal stresses. Also, note that since the shear modulus μ (see Eq. (88)) and the density ρ depend on the state of the material, the value of the Rayleigh wave speed is pressure dependent.

3.2.2. Crack nucleation

New cracks are presumed to be in a range of sizes with the same size distribution given by Eq. (11a). According to the proposed model there are two reasons for crack nucleation:

1. Crack branching.
2. Generation due to pore crushing.

At present it is not known whether the limiting crack growth speed is the cause for crack branching or whether crack branching is the cause for the limiting crack growth speed. For either case, the following physical reasoning seems to be applicable. As loads are applied, the magnitude of the crack's driving force (energy release rate G_i) rises. When a critical value G_C is exceeded, the crack starts to grow at the rate controlled by Eq. (19a). As the limiting speed is approached and more energy is applied (because of external loads) it is no longer possible to dissipate this energy by growing a single crack and crack branching (i.e. nucleation) occurs. Here, $\hat{n}_b$ is a function that characterizes the "generation/nucleation" of new cracks due to the branching process

$$\hat{n}_b = \kappa_3 n \frac{\langle G_i - G_C \rangle}{G_C} C_R. \tag{20}$$

Another source for new cracks is due to the crushing of pores during compressive loading. When the pressure rises above a threshold pressure p_{crush}, pores start to crush, creating new cracks at the pore's surface that penetrate into the solid (this is in contrast with the behavior of pores in a ductile material, where the pore volume is assumed to decrease with no cracking). The rate of crack generation due to pore crushing is given by

$$\hat{n}_C = \kappa_4 \phi \left[1 - \exp\left[- \left(\frac{\langle p - p_{crush} \rangle}{p_{crush}} \right)^{\kappa_5} \right] \right] C_R. \tag{21}$$

In these formulae, κ_3, κ_4 have units of m^{-1} and κ_5 is unitless. These material parameters are determined by comparing model results with experimental data.

Moreover, combining these expressions, an evolution equation for the number of cracks is proposed which depends on the rate of branching $\hat{n}_b$ and on the rate of pore crushing $\hat{n}_C$, such that

$$\dot{n} = \hat{n}_b + \hat{n}_C. \tag{22}$$

3.3. Integrity

The notions of failure and damage should not be confused. Failure means the inability of the material to sustain stress, or the inability of the whole structure to sustain load, whereas damage might describe the fraction of flawed volume in the RVE. To emphasize the difference between these concepts, it is clear that the RVE is going to fail a long time before it is completely damaged.

The usual models of damage assume that the material moduli monotonically decrease with increasing damage. However, it is known from experience that when a material is compacted (closure/collapse of pores) these moduli tend to become larger than their unloaded values. Consequently, a general model is needed to describe this modulus enhancement. For this reason, it is convenient to introduce the integrity (I) of the material in the RVE as

$$I = \frac{\text{Modulus}(t)}{\text{Reference solid modulus}}. \tag{23}$$

In theoretical models for moduli degradation (e.g. Budiansky and O'Connell, 1976; Horii and Nemat-Nasser, 1983; Margolin, 1983), the effective moduli are determined through an equation which defines the effective strain tensor as the sum of the elastic strain and the strain due to crack formation. The result of this equation is a general expression for the moduli degradation due to cracks in the material of the form

$$\frac{\text{Modulus}(t)}{\text{Reference solid modulus}} = \frac{1}{1 + R(v)\zeta_C}, \quad \zeta_C = n\bar{a}^3, \tag{24a, b}$$

where $R(v)$ is an expression that depends on the specific degraded modulus, and ζ_C is the crack "density".

An expression for a mixture of spherical cavities and randomly oriented penny-shaped cracks is found in Kachanov (1993) and Kachanov et al. (1994), which suggests that the integrity takes the form

$$\frac{\text{Modulus}(t)}{\text{Reference solid modulus}} = \frac{1 - \phi}{1 - \phi + c_0\phi + c_1\zeta_C}, \tag{25}$$

where ϕ is the porosity (see Eq. (40a)), and c_0 and c_1 are constants. As a special case when $c_0 = 1$, this expression yields

$$\frac{\text{Modulus}(t)}{\text{Reference solid modulus}} = \frac{1 - \phi}{1 + c_1\zeta_C}. \tag{26}$$

Obviously, when the porosity vanishes ($\phi = 0$) and $c_1 = R(v)$, the expression for the integrity (26) reduces to Eq. (24a).

The objective of this section is to generalize Eq. (26) to include the effect of varying stress states on the expression for the integrity of the shear modulus. To this end, it might seem appropriate to take c_1 in (26) to be an explicit function of stress, such that

$$\frac{\text{Modulus}(t)}{\text{Reference solid modulus}} = \frac{1 - \phi}{1 + A_C\zeta_C}, \tag{27}$$

where the expression $R(v)$ is replaced by A_C for generality. This value A_C should include the effect of friction on the degradation of the moduli and the effect of varying stress states. Also, when all cracks are open (all principal stresses are positive) A_C should equal $R(v)$.

However, in the present development, the integrity I appears explicitly in the functional form for the Helmholtz free energy. Moreover, the stress is determined by a derivative of the Helmholtz free energy. Consequently, it is quite inconvenient for I to depend directly on stress. To avoid this difficulty, the integrity is proposed in the form

$$I(D_C, \phi) = \frac{1 - \phi}{1 + D_C}, \tag{28}$$

where D_C is a new history-dependent variable which represents a measure of damage in the material due to crack formation. Specifically, D_C is determined by integrating the evolution equation

$$\dot{D}_C = A_C\dot{\zeta}_C. \tag{29}$$

Since the crack density ζ_C can only increase, it follows that the damage variable D_C can only increase in response to crack nucleation and growth. When A_C is a constant, then (29) integrates to obtain common results like (27). However, the evolution Eq. (29) has the advantage that A_C can be an arbitrary unitless nonnegative function of stress without complicating the functional form of the Helmholtz free energy. This means that A_C can be used to model the dependence of the integrity I on the history of stress. Moreover, the expression (28) for the integrity has the physical property that it tends to increase when porosity ϕ decreases.

The expression for A_C in the general case is motivated by first considering two simple cases where I and A_C can be determined analytically in closed form from linear elasticity:

Case 1: All cracks are open (i.e. all principal stresses are positive). Using the expression (Keer, 1966; Sneddon, 1969)

$$u_N = \frac{4(1-\nu^2)}{\pi E}\sigma_N\sqrt{a^2-r^2}, \tag{30a}$$

for the normal displacement, and the expression (Segedin, 1950; Keer, 1966)

$$u_T = \frac{4(1-\nu)}{\pi E(2-\nu)}\sigma_T\sqrt{a^2-r^2}, \tag{30b}$$

for the tangential displacement, it follows that Eq. (6.6.14a) in Nemat-Nasser and Hori (1993) can be written in the form of their Eq. (6.6.14c) such that

$$I = \frac{\mu}{\mu_0} = \frac{1}{1+f\left[\frac{32(1-\nu)(5-\nu)}{45(2-\nu)}\right]}, \tag{31}$$

where f is defined as in their Eq. (6.6.10a) by

$$f \equiv \int a^3 w_a \,\mathrm{d}a = \frac{\pi}{2} n\bar{a}^3 = \frac{\pi}{2}\zeta_C. \tag{32}$$

The factor $\pi/2$, which is the only difference between the value of f in (32) and its value in Eq. (6.6.10d) in Nemat-Nasser and Hori (1993), is due solely to the different crack distribution function w_a used here. Consequently, the expression (28) for zero porosity ($\phi = 0$) will give the same results as (31) if A_C in (29) is specified by the constant

$$A_C^1 = \frac{\pi}{2}\left[\frac{32(5-\nu)(1-\nu)}{45(2-\nu)}\right]. \tag{33}$$

Case 2: All cracks are closed (i.e. all principal stresses are negative) and friction between the crack faces is neglected. In this case, the same procedure is followed as described in Case 1. However, the normal displacement vanishes ($u_N = 0$), and the tangential displacement is given by Segedin (1950)

$$u_T = \frac{8(1-\nu^2)}{\pi E(2-\nu)}\sigma_T\sqrt{a^2-r^2}, \tag{34}$$

which yields the result that

$$I = \frac{\mu}{\mu_0} = \frac{1}{1+f\left[\frac{96(1-\nu)}{45(2-\nu)}\right]}. \tag{35}$$

As in Case 1, the expression (28) for zero porosity ($\phi = 0$) gives the same result as (35) if A_C in (29) is specified by the constant

$$A_C^2 = \frac{\pi}{2}\left[\frac{96(1-\nu)}{45(2-\nu)}\right]. \tag{36}$$

General Case: For a general state of stress the response of the solid is not so simple since for some crack orientations $\sigma_N > 0$ and the crack is open, whereas for other orientations $\sigma_N \leqslant 0$ and the crack is closed. Moreover, the influence of friction on the tangential displacement should be included. To describe this more complicated situation it is convenient to recall that the principle stresses σ_i can be ordered ($\sigma_1 \geqslant \sigma_2 \geqslant \sigma_3$) so that the normal stress $\sigma = (\sigma_1 + \sigma_3)/2$ and the shear stress $\tau = (\sigma_1 - \sigma_3)/2$ act on the plane of maximum shear stress. Also, it is convenient to introduce the auxiliary variables ξ_1 and ξ_2 by the expressions

$$\xi_1 = \frac{\langle -\sigma_3 \rangle}{\langle \sigma_1 \rangle + \langle -\sigma_3 \rangle}, \quad 0 \leqslant \xi_1 \leqslant 1, \tag{37a, b}$$

$$\xi_2 = \frac{\langle \tau - f_C \langle -\sigma \rangle \rangle}{\tau_s + \langle \tau - f_C \langle -\sigma \rangle \rangle}, \quad 0 \leqslant \xi_2 \leqslant 1, \tag{37c, d}$$

where τ_s is a positive material constant. Then the functional form for A_C for the General Case is proposed by

$$A_C = (1 - \xi_1)A_C^1 + \xi_1\xi_2 A_C^2. \tag{38}$$

This function has the properties that it includes the limiting Case 1 ($A_C = A_C^1$) when all cracks are open ($\sigma_3 > 0$, with $\xi_1 = 0$) and the limiting Case 2 ($A_C = A_C^2$) when all cracks are closed ($\sigma_1 < 0$ with $\xi_1 = 1$) with near full slip occurring $[\tau - f_C\langle -\sigma \rangle] \gg \tau_s$. It also includes the case of no slip ($A_C = 0$) when all cracks are closed ($\sigma_1 < 0$, with $\xi_1 = 1$) and the shear stress is below the slip threshold $[\tau < f_C\langle -\sigma \rangle]$.

4. Porosity

In many constitutive models, a RVE dv of brittle material in the present configuration (at time t) is decomposed into a solid part whose volume is dv_s and a pore volume dv_p, such that

$$dv = dv_s + dv_p, \quad dV = dV_S + dV_P, \tag{39a, b}$$

where dV, dV_S, dV_P are the values of dv, dv_s, dv_p in a fixed-reference configuration, and the indexes s, p denote the solid and pores, respectively. The porosity ϕ and its reference value Φ are then defined by

$$\phi = \frac{dv_p}{dv}, \quad \Phi = \frac{dV_P}{dV}. \tag{40a, b}$$

The relative volume is a nondimensional expression that describes the ratio between the volume of the RVE in the present configuration and its volume in the reference configuration. Thus, for the total volume and for the solid part, it follows that

$$J = \frac{dv}{dV}, \quad J_s = \frac{dv_s}{dV_S}, \quad \rho_0 = (1 - \Phi)\rho_{s0}, \quad \rho = (1 - \phi)\rho_s, \tag{41a–d}$$

where ρ is the density in the present configuration, ρ_s is the solid density in the present configuration, ρ_{s0} is the solid density in the reference configuration, and use has been made of the conservation of mass equation ($\rho J = \rho_0$).

Next, with the help of Eqs. (40) and (41) it can be shown that

$$J_s = \frac{1-\phi}{1-\Phi} J. \tag{42}$$

Moreover, since the total relative volume J is determined by the evolution equation

$$\dot{J} = J(\mathbf{D}\cdot\mathbf{I}), \tag{43}$$

it follows that the solid relative volume J_s is determined by

$$\dot{J}_s = J_s\left[(\mathbf{D}\cdot\mathbf{I}) - \frac{1}{1-\phi}\dot{\phi}\right]. \tag{44}$$

The continuum model assumes that stresses are uniform throughout the RVE. This assumption ignores the effect of stress concentrations near pores in the solid matrix and seems to predict an elastic response that is too stiff. To remedy this problem, the added elastic compressibility observed in the porous material is modeled (following Rubin et al., 1996), by proposing a function for the porosity ϕ such that the total porosity is

$$\phi = \hat{\phi}(J,\theta,\phi_u,D_C). \tag{45}$$

Here, D_C is the crack damage parameter that was defined in Section 3, ϕ_u is the porosity of the material in the unloaded state ($\theta=\theta_0$, $\mathbf{T}=0$), which is calculated by integrating an evolution equation, and the corresponding value of the total relative volume J in the unloaded state is denoted by J_u, using Eq. (42) [with $J_s=1$ for $\phi=\phi_u$ and $J=J_u$]

$$J_u = \frac{1-\Phi}{1-\phi_u}. \tag{46}$$

Differentiating the porosity function ϕ with respect to time yields

$$\dot{\phi} = \frac{\partial\hat{\phi}}{\partial J}\dot{J} + \frac{\partial\hat{\phi}}{\partial\theta}\dot{\theta} + \frac{\partial\hat{\phi}}{\partial\phi_u}\dot{\phi}_u + \frac{\partial\hat{\phi}}{\partial D_C}\dot{D}_C. \tag{47}$$

For expanded states ($J > J_u$), the value of porosity $\phi_s(J,\theta)$ associated with zero pressure is given by

$$\phi_s(J,\theta) = 1 - \left(\frac{1-\Phi}{J}\right)F_s(\theta). \tag{48}$$

Here $F_s(\theta)$ is the value of the relative volume of the solid J_s that causes the part of the pressure $p_{s1}(J_s,\theta)$ (see Eq. (77)) associated with changes of density and temperature to vanish.

It is assumed that the solid matrix is rather brittle so that it cannot sustain a significant negative value of pressure without creating substantial increase in porosity. Thus, it is expected that in expanded states ($J > J_u$) the value of the solid relative volume J_s will remain close to the value of $F_s(\theta)$ as the material dilates. To model both compressed and expanded states, the functional form for the porosity is specified as

$$\hat{\phi}(J,\theta,\phi_u,D_C) = \phi(\phi_u,\phi_s) = \left\{\begin{array}{ll} \phi_u & \text{for } \phi_u \geqslant \phi_s \\ \phi_s - b_s^t(1-\phi_s)\tanh\left[\frac{(\phi_s-\phi_u)}{b_0^t(1-\phi_s)}\right] & \text{for } \phi_u < \phi_s \end{array}\right\}, \tag{49a, b}$$

$$b_s^t = \frac{1}{1+D_C} b_0^t. \tag{49c}$$

Here, b_0^t is a material constant to be found through calibration and the value of b_s^t decreases as cracks grow and nucleate.

4.1. Evolution of the unloaded porosity

The porosity ϕ is determined by (49) which depends on the current material state being compressed (49a) or expanded (49b), according to the relative values of the two porosity variables ϕ_s and ϕ_u. In the following, it is convenient to define the minimum value $\phi_u^{\min}$ of ϕ_u for all time by

$$\phi_u^{\min} = \mathrm{Min}[\phi_u]. \tag{50}$$

Sometimes the evolution equations for porosity are formulated in terms of compaction and dilation surfaces, which remain zero during compaction or dilation, respectively. However, since the dependence of the pressure on the porosity can be quite nonlinear, these equations are "stiff" and the iterative procedures used to solve them can cause numerical instabilities in the computer code. To eliminate most of these numerical difficulties, the constitutive equations for the unloaded porosity ϕ_u are formulated as rate-independent evolution equations of the forms

For $(\mathbf{D}\cdot\mathbf{I}) < 0$:

$$\dot{\phi}_u = \left\{ \begin{array}{ll} f_3(p)(\mathbf{D}\cdot\mathbf{I}) & \text{for } p > p_{\mathrm{crush}} \\ \dfrac{1-\Phi}{J}(\mathbf{D}\cdot\mathbf{I})H(\phi_u - \phi_u^{\min}) & \text{for } p_{\mathrm{crush}} \geqslant p \geqslant 0 \\ 0 & \text{for } p < 0 \end{array} \right\} \tag{51a–c}$$

and for $(\mathbf{D}\cdot\mathbf{I}) \geqslant 0$:

$$\dot{\phi}_u = \left\{ \begin{array}{ll} 0 & \text{for } p > -p_d \\ C_3\langle\phi_s - \phi_u\rangle(\mathbf{D}\cdot\mathbf{I}) & \text{for } p \leqslant -p_d \end{array} \right\}, \tag{52a, b}$$

where $H(x)$ is the Heavyside function defined by

$$H(x) = 0 \quad \text{for } x \leqslant 0, \qquad H(x) = 1 \quad \text{for } x > 0. \tag{53}$$

Here p_{crush} is a threshold pressure to begin pore collapse in compaction, C_3 is a material parameter to be determined, and p_d is a threshold magnitude of the tensile pressure at the onset of unloaded porosity growth in dilation, which is degraded by loss of integrity

$$p_d = p_d^0 I. \tag{54}$$

Also, $f_3(p)$ is given by

$$f_3(p) = \left[C_1\left(\frac{p - p_{\mathrm{crush}}}{p_{\mathrm{crush}}}\right) + C_2\left(\frac{p - p_{\mathrm{crush}}}{p_{\mathrm{crush}}}\right)^2 \right], \tag{55}$$

where C_1, C_2 are material constants to be determined.

It is obvious that the pressure cannot be the sole measure used to define the domains for porous compaction ($\dot{\phi}_u < 0$) and porous dilation ($\dot{\phi}_u > 0$). For example, for a fixed value of pressure $p > p_{\mathrm{crush}}$, porous compaction (51a) occurs if the material is being compressed ($\mathbf{D}\cdot\mathbf{I} < 0$), whereas ϕ_u remains constant (52a) if the material is being expanded ($\mathbf{D}\cdot\mathbf{I} > 0$). Porous dilation also occurs during expansion with negative pressure (52b) as voids grow and gaps form between fragments of material. During recompression from this dilated state, the gaps are closed with negligible increase in pressure since (51b) causes J_s to remain constant.

5. Constitutive equations for the intact material

Before developing a set of constitutive equations for a material full of cracks and pores, it is convenient to postulate the HFE for a "virgin" intact material, following the work of Rubin et al. (1996). The subscript s in any variable refers to the solid constituent in a composite material, which in this case is the only constituent

$$\psi(J_s,\theta,\alpha_1)=\psi_{s1}(J_s,\theta)+\psi'_s(J_s,\theta,\alpha_1), \tag{56a}$$

$$\rho_{s0}\psi_{s1}(J_s,\theta)=\rho_{s0}C_v\left[(\theta-\theta_0)-\theta\ln\left(\frac{\theta}{\theta_0}\right)\right]-(\theta-\theta_0)f_1(J_s)+f_2(J_s), \tag{56b}$$

$$\rho_{s0}\psi'_s(J_s,\theta,\alpha_1)=\tfrac{1}{2}\hat{\mu}_s(J_s,\theta)(\alpha_1-3), \tag{56c}$$

where θ_0 is the reference temperature and $\mu_s(J_s,\theta)$ is the shear modulus of the solid which depends on the relative volume and the temperature of the solid (e.g. Steinberg, 1991).

The first part ψ_{s1} of the HFE characterizes the response to dilatational deformations and is a function of J_s and θ only. In this expression, C_v is the specific heat at constant volume and distortional deformation (which can be temperature dependent but is taken here to be constant) and f_1, f_2 are functions of J_s to be determined later.

The second part ψ'_s of the HFE characterizes the response of the material to distortional deformation. The symmetric tensor $\mathbf{B}'_e$ is a pure measure of elastic distortional deformation (Rubin and Attia, 1996) which is determined by the evolution equation

$$\dot{\mathbf{B}}'_e=\mathbf{L}\mathbf{B}'_e+\mathbf{B}'_e\mathbf{L}^{\mathrm{T}}-\tfrac{2}{3}(\mathbf{D}\cdot\mathbf{I})\mathbf{B}'_e-\Gamma\tilde{\mathbf{A}},\quad \det[\mathbf{B}'_e]=1, \tag{57a, b}$$

where

$$\tilde{\mathbf{A}}=\mathbf{B}'_e-\left[\frac{3}{\mathbf{B}'^{-1}_e\cdot\mathbf{I}}\right]\mathbf{I}. \tag{58}$$

The symmetric tensor $\tilde{\mathbf{A}}$ characterizes the relaxation effects of plasticity on the evolution of elastic distortional deformation, and the function Γ is a nonnegative function determined using a consistency condition for rate-independent plasticity (Rubin and Attia, 1996).

The scalar α_1 is one of the two independent nontrivial invariants of the elastic distortional deformation $\mathbf{B}'_e$, which can be written as

$$\alpha_1=\mathbf{B}'_e\cdot\mathbf{I}\quad\text{and}\quad\alpha_2=\mathbf{B}'_e\cdot\mathbf{B}'_e. \tag{59}$$

Here, for simplicity, the Helmholtz free energy is taken to be independent of α_2. Also, the time derivative of α_1 is given by

$$\dot{\alpha}_1=2\left[\mathbf{B}'_e-\tfrac{1}{3}(\mathbf{B}'_e\cdot\mathbf{I})\mathbf{I}\right]\cdot\mathbf{D}-\Gamma(\mathbf{I}\cdot\tilde{\mathbf{A}}) \tag{60}$$

For the solid material with no pores, $\psi=\psi_s$ and $\phi=\Phi=0$, so that with the help of (41), (42), (44), (56) and (60), the reduced balance of energy Eq. (8) can be written in the form

$$\left[\rho_{s0}\eta-\rho_{s0}C_v\ln(\theta/\theta_0)-f_1(J_s)+\frac{1}{2}\frac{\partial\hat{\mu}_s(J_s,\theta)}{\partial\theta}(\alpha_1-3)\right]\dot{\theta}+\left\{-J_s\mathbf{T}+J_s\left[-(\theta-\theta_0)\frac{df_1}{dJ_s}+\frac{df_2}{dJ_s}+\frac{1}{2}\frac{\partial\hat{\mu}_s(J_s,\theta)}{\partial J_s}(\alpha_1-3)\right]\mathbf{I}+\hat{\mu}_s(J_s,\theta)\left[\mathbf{B}'_e-\frac{1}{3}(\mathbf{B}'_e\cdot\mathbf{I})\mathbf{I}\right]\right\}\cdot\mathbf{D}+\left[\rho_{s0}\theta\xi'-\frac{1}{2}\hat{\mu}_s(J_s,\theta)\Gamma\tilde{\mathbf{A}}\cdot\mathbf{I}\right]=0 \tag{61}$$

Now, within the context of the thermodynamic developments of Green and Naghdi (1977, 1978), the constitutive equations must be restricted so that Eq. (61) is satisfied for all thermomechanical processes. For elastic–plastic solids of the type considered in this section, the necessary and sufficient conditions for this to be satisfied yield the following constitutive equations. The specific entropy is given by

$$\eta=\eta_s=-\frac{\partial\psi_s}{\partial\theta}=\eta_{s1}(J_s,\theta)+\eta'_s(J_s,\theta), \tag{62a}$$

$$\eta_{s1}=C_v\ln\left(\frac{\theta}{\theta_0}\right)+\frac{1}{\rho_{s0}}f_1(J_s),\quad \eta'_s=-\frac{1}{2\rho_{s0}}\frac{\partial\hat{\mu}_s}{\partial\theta}(\alpha_1-3) \tag{62b, c}$$

and the specific entropy η_s vanishes in the reference configuration ($J_s=1,\theta=\theta_0,\mathbf{B}'_e=\mathbf{I}$). The specific internal energy ε_s is given by

$$\varepsilon=\varepsilon_s=(\hat{\psi}_s+\theta\hat{\eta}_s)=\varepsilon_{s1}+\varepsilon'_s, \tag{63a}$$

$$\varepsilon_{s1}=C_v(\theta-\theta_0)+\frac{\theta_0}{\rho_{s0}}f_1(J_s)+\frac{1}{\rho_{s0}}f_2(J_s), \tag{63b}$$

$$\varepsilon'_s=\frac{1}{2\rho_{s0}}\left[\hat{\mu}_s-\theta\frac{\partial\hat{\mu}_s}{\partial\theta}\right](\alpha_1-3). \tag{63c}$$

The rate of dissipation due to distortional plastic deformation is given by

$$\rho_{s0}\theta\xi'=\rho_{s0}\theta\xi'_d=\tfrac{1}{2}\hat{\mu}_s(J_s,\theta)\Gamma(\mathbf{I}\cdot\tilde{\mathbf{A}}), \tag{64}$$

and the Cauchy stress separates into a pressure p and a deviatoric part $\mathbf{T}'$, such that

$$\mathbf{T}=-p\mathbf{I}+\mathbf{T}',\quad \mathbf{T}'\cdot\mathbf{I}=0, \tag{65a, b}$$

where for the material under consideration

$$\mathbf{T}=\mathbf{T}_s=-p_s\mathbf{I}+\mathbf{T}'_s, \tag{66a}$$

$$\mathbf{T}'=\mathbf{T}'_s=\frac{\hat{\mu}_s(J_s,\theta)}{J_s}\left[\mathbf{B}'_e-\frac{1}{3}(\mathbf{B}'_e\cdot\mathbf{I})\mathbf{I}\right], \tag{66b}$$

$$p=p_s=-\rho_{s0}\frac{\partial\psi_s}{\partial J_s}=p_{s1}(J_s,\theta)+p'_s(J_s,\theta,\alpha_1), \tag{66c}$$

$$p_{s1}=(\theta-\theta_0)\frac{df_1(J_s)}{dJ_s}-\frac{df_2(J_s)}{dJ_s},\quad p'_s(J_s,\theta)=-\frac{1}{2}\frac{\partial\hat{\mu}_s}{\partial J_s}(\alpha_1-3). \tag{66d, e}$$

In these constitutive equations, the parts $\{\psi_{s1},\eta_{s1},\varepsilon_{s1},p_{s1}\}$ characterize the thermomechanical response to dilatational deformation, whereas the other parts include the effects of distortional elastic deformation.

Many constitutive models for shock waves assume that the pressure is determined by a Mie–Grüneisen equation of state. For such models, it has been assumed (Rubin, 1986) that p_{s1} is related to ε_{s1} by the formula

$$p_{s1} = p_{sH}(J_s) + \rho_{s0}\frac{\gamma_s(J_s)}{J_s}[\varepsilon_{s1} - \varepsilon_{sH}(J_s)], \tag{67}$$

where $\gamma(J_s)$ is the Grüneisen gamma, which controls the temperature dependence of the pressure, p_{sH} and ε_{sH} are the pressure and the internal energy associated with the Hugoniot of the solid material

$$p_{sH}(J_s) = \rho_{s0}U_s^2(1 - J_s), \tag{68a}$$

$$\varepsilon_{sH}(J_s) = \frac{p_{sH}(J_s)(1 - J_s)}{2\rho_{s0}}. \tag{68b}$$

U_s is the shock velocity, and $\gamma(J_s)$ is given by

$$\gamma_s(J_s) = \gamma_0 J_s, \tag{69}$$

which is a common assumption in many shock-wave codes. Also, U_s is taken in the form

$$U_s = \left\{ \begin{array}{ll} \dfrac{C_0}{1 - S_1(1 - J_s) - S_2(1 - J_s)^2 - S_3(1 - J_s)^3} & \text{for } J_s \leqslant 1 \\ \dfrac{C_0}{[1 - (\gamma_{s0}/2)(1 - J_s)]^{1/2}} & \text{for } J_s > 1 \end{array} \right\}, \tag{70}$$

where γ_0, S_1, S_2, S_3 are material constants.

Moreover, using Rubin (1986) it can be shown that the constitutive relations (Eqs. (62)–(66) are consistent with the Mie–Grüneisen form (Eq. (67)), provided that f_1 and f_2 satisfy the differential equations

$$\frac{\mathrm{d}f_1(J_s)}{\mathrm{d}J_s} = \rho_{s0}C_v\frac{\gamma_s(J_s)}{J_s}, \tag{71a}$$

$$\frac{\mathrm{d}f_2(J_s)}{\mathrm{d}J_s} + \frac{\gamma_s(J_s)}{J_s}f_2(J_s) = -p_{sH}(J_s) + \rho_{s0}\frac{\gamma_s(J_s)}{J_s}\varepsilon_{sH}(J_s) - \theta_0\frac{\gamma_s(J_s)}{J_s}f_1(J_s). \tag{71b}$$

Substituting Eqs. (68a,b) into Eqs. (71a,b) and using the conditions that

$$f_1 = 0, \quad f_2 = 0, \quad \frac{\mathrm{d}f_2}{\mathrm{d}J_s} = 0 \quad \text{for } J_s = 1 \tag{72a–c}$$

the solution of (71a,b) can be represented in the forms

$$f_1(J_s) = -\rho_{s0}C_v\gamma_0(1 - J_s), \tag{73a}$$

$$f_2(J_s) = \mathrm{e}^{-\gamma_0 J_s}\int_{1.0}^{J_s}\mathrm{e}^{\gamma_0 x}[-p_{sH}(x) + \rho_{s0}\gamma_0\varepsilon_{sH}(x) - \theta_0\gamma_0 f_1(x)]\,\mathrm{d}x. \tag{73b}$$

Here, the function f_2 is determined numerically and values are stored in a table for future use.

Next, the function $F_s(\theta)$ is defined which is the value of the relative volume of the solid J_s that will cause the pressure $p_{s1}(J_s, \theta)$ in Eq. (66d) to vanish, so that

$$p_{s1}(J_s, \theta) = 0 \quad \text{when } J_s = F_s(\theta). \tag{74}$$

Also, it is assumed that $F_s(\theta_0) = 1$ in the reference configuration, which is stress free, with $J_s = 1$. To find the expression for $p_{s1}(J_s, \theta)$, Eq. (63b) is solved for $(\theta - \theta_0)$

$$(\theta-\theta_0)=\frac{1}{\rho_{s0}C_v}[\rho_{s0}\varepsilon_{s1}-\theta_0 f_1(J_s)-f_2(J_s)] \tag{75}$$

and the result is substituted into Eq. (66d) to yield

$$p_{s1}=\frac{1}{\rho_{s0}C_v}[\rho_{s0}\varepsilon_{s1}-\theta_0 f_1(J_s)-f_2(J_s)]\frac{df_1}{dJ_s}-\frac{df_2}{dJ_s}. \tag{76}$$

Thus, with the help of Eq. (67), the pressure in the solid takes the form

$$p_{s1}(J_s,\theta)=\rho_{s0}\gamma_0\left[C_v(\theta-\theta_0)+\frac{\theta_0}{\rho_{s0}}f_1+\frac{1}{\rho_{s0}}f_2-\varepsilon_{sH}(J_s)\right]+p_{sH}(J_s). \tag{77}$$

For a brittle material, the value of J_s is always close to 1.0, since the material cannot sustain significant tensile stress. This fact is used to simplify Eq. (77), by using a Taylor expansion

$$p_{s1}(J_s,\theta)=p_{s1}(1,\theta)+\frac{\partial p_{s1}}{\partial J_s}(1,\theta)(J_s-1)+\cdots, \tag{78}$$

$$p_{s1}(J_s,\theta)=\gamma_0\rho_{s0}C_v(\theta-\theta_0)-[\rho_{s0}C_0^2-\gamma_0^2\rho_{s0}C_v\theta_0](J_s-1)+\cdots \tag{79}$$

Then, substituting Eq. (74) into Eq. (79) yields

$$0\cong\gamma_0\rho_{s0}C_v(\theta-\theta_0)-(\rho_{s0}C_0^2-\gamma_0^2\rho_{s0}C_v\theta_0)[F_s(\theta)-1], \tag{80}$$

which can be used to obtain the result that

$$F_s(\theta)\cong 1+B_{eqv}(\theta-\theta_0),\quad B_{eqv}=\frac{\gamma_0\rho_{s0}C_v}{\rho_{s0}C_0^2-\gamma_0^2\rho_{s0}C_v\theta_0}. \tag{81a, b}$$

The coefficient B_{eqv} is very small (on the order of a few hundredths). Consequently, unless the temperature of the solid is very high, $F_s(\theta)$ remains close to unity.

6. Constitutive equations for cracked and porous material

To model the response of a fractured porous material it is assumed that the HFE ψ is related to the functional form (56) of ψ_s for the nonporous solid. Here, it is of interest to modify the form (56) slightly by including the degradation of the shear modulus due to crack growth and nucleation. Therefore, for the present model, ψ is proposed in the form

$$\begin{aligned}&\rho_0\psi(J_s,\theta,\alpha_1,D_C,\psi_C)\\&\quad=(1-\Phi)\left\{\rho_{s0}C_v\left[(\theta-\theta_0)-\theta\ln\left(\frac{\theta}{\theta_0}\right)\right]-(\theta-\theta_0)f_1(J_s)+f_2(J_s)+\frac{1}{2}\frac{\hat{\mu}_s(J_s,\theta)}{(1+D_C)}(\alpha_1-3)\right\}.\end{aligned} \tag{82}$$

In order to develop the restrictions on the constitutive equations for this fractured porous material, it is convenient to use the expressions (41), (42), (44), (47) and (60)–(62) to determine the derivative of the expression (82) for the HFE. This result can be used to rewrite the balance of energy (8) in the form

$$\left[\rho_0\eta-\rho_0\eta_{\mathrm{s}}^c+Jp_{\mathrm{s}}^c\frac{\partial\hat{\phi}}{\partial\theta}\right]\dot{\theta}+J\left\{-\left[1-\phi-J\frac{\partial\hat{\phi}}{\partial J}\right]p_{\mathrm{s}}^c\mathbf{I}+\frac{1-\phi}{1+D_{\mathrm{C}}}\mathbf{T}_{\mathrm{s}}'-\hat{\mathbf{T}}\right\}\cdot\mathbf{D}$$
$$+\rho_0\theta\xi'-\frac{(1-\Phi)}{2}\frac{\hat{\mu}_{\mathrm{s}}(J_{\mathrm{s}},\theta)}{1+D_{\mathrm{C}}}\Gamma(\mathbf{I}\cdot\tilde{\mathbf{A}})+Jp_{\mathrm{s}}^c\frac{\partial\hat{\phi}}{\partial\phi_{\mathrm{u}}}\dot{\phi}_{\mathrm{u}}+\left[Jp_{\mathrm{s}}^c\frac{\partial\hat{\phi}}{\partial D_{\mathrm{C}}}-\frac{(1-\Phi)}{2(1+D_{\mathrm{C}})}\frac{\hat{\mu}_{\mathrm{s}}(J_{\mathrm{s}},\theta)}{1+D_{\mathrm{C}}}(\alpha_1-3)\right]\dot{D}_{\mathrm{C}}=0, \tag{83}$$

where the following auxiliary parameters have been defined for convenience

$$\eta_{\mathrm{s}}^c=\eta_{\mathrm{s1}}+\frac{1}{1+D_{\mathrm{C}}}\eta_{\mathrm{s}}',\quad p_{\mathrm{s}}^c=p_{\mathrm{s1}}+\frac{1}{1+D_{\mathrm{C}}}p_{\mathrm{s}}'. \tag{84}$$

It then follows that the constitutive equations

$$\rho_0\eta=(1-\Phi)\rho_{\mathrm{s0}}\eta_{\mathrm{s}}^c-Jp_{\mathrm{s}}^c\frac{\partial\hat{\phi}}{\partial\theta}, \tag{85a}$$

$$\hat{p}=p_{\mathrm{s}}^c\left[1-\phi-J\frac{\partial\hat{\phi}}{\partial J}\right],\quad \mathbf{T}'=\frac{1-\phi}{1+D_{\mathrm{C}}}\mathbf{T}_{\mathrm{s}}'=I\mathbf{T}_{\mathrm{s}}', \tag{85b, c}$$

$$\xi'=\xi_{\mathrm{d}}'+\xi_{\phi}'+\xi_{\mathrm{C}}', \tag{85d}$$

$$\rho_0\theta\xi_{\mathrm{d}}'=\frac{1}{2}\frac{J}{J_{\mathrm{s}}}I\hat{\mu}_{\mathrm{s}}(J_{\mathrm{s}},\theta)\Gamma(\mathbf{I}\cdot\tilde{\mathbf{A}}), \tag{85e}$$

$$\rho_0\theta\xi_{\phi}'=-Jp_{\mathrm{s}}^c\frac{\partial\hat{\phi}}{\partial\phi_{\mathrm{u}}}\dot{\phi}_{\mathrm{u}}, \tag{85f}$$

$$\rho_0\theta\xi_{\mathrm{C}}'=\left[-Jp_{\mathrm{s}}^c\frac{\partial\hat{\phi}}{\partial D_{\mathrm{C}}}+\frac{1}{2(1+D_{\mathrm{C}})}\frac{J}{J_{\mathrm{s}}}I\mu_{\mathrm{s}}(J_{\mathrm{s}},\theta)(\alpha_1-3)\right]\dot{D}_{\mathrm{C}}, \tag{85g}$$

represent sufficient conditions for the energy Eq. (8) to be satisfied for all thermomechanical processes. In these constitutive equations the expression (85e) for ξ_{d}' has been modified relative to (64) to include the effect of the loss of integrity due to crack growth and nucleation. Also, the specific internal energy ε of the fractured porous material is given by

$$\varepsilon=\psi+\theta\eta. \tag{86}$$

Thus, with the help of (62), (63) and (82) it can be shown that

$$\rho_0\varepsilon=\rho_0C_v(\theta-\theta_0)+(1-\Phi)(\theta_0f_1+f_2)+\frac{(1-\Phi)}{2(1+D_{\mathrm{C}})}\left[\mu_{\mathrm{s}}-\theta\frac{\partial\mu_{\mathrm{s}}}{\partial\theta}\right](\alpha_1-3)-Jp_{\mathrm{s}}^c\theta\frac{\partial\hat{\phi}}{\partial\theta}. \tag{87}$$

Also, it can be seen from (66b) and (85c) that the effective shear modulus is given by

$$\mu=I\frac{\hat{\mu}_{\mathrm{s}}}{J_{\mathrm{s}}}. \tag{88}$$

The statement (10) of the second law of thermodynamics requires the material dissipation ξ' to be nonnegative. Although, only the sum (85d) need be nonnegative, it will presently be shown that under most situations each of the terms ξ_{d}', ξ_{ϕ}' and ξ_{C}' is nonnegative by itself. In this regard, it follows directly from the work in Rubin et al. (2000) that the terms ξ_{d}' and $(\partial\hat{\phi}/\partial\phi_{\mathrm{u}})$ are each nonnegative, and that p_{s}^c has the same

sign as the total pressure p. Thus, it follows from the evolution equations for the unloaded porosity ϕ_u that for nonnegative pressure, ϕ_u either decreases (51a,b) or remains constant (52a). Similarly, for negative pressure, ϕ_u either remains constant ((51c), (52a)), or increases (52b). This means that the dissipation term ξ'_ϕ is nonnegative.

Furthermore, with regard to the term ξ'_C, it follows from (49) that $(\partial\hat{\phi}/\partial D_C)$ vanishes for $\phi_u \geqslant \phi_s$ (corresponding to nonnegative pressure p_{s1}) and that it is nonnegative for $\phi_u < \phi_s$ (corresponding to negative pressure p_{s1}). Moreover, since $\alpha_1 \geqslant 3$ and the shear modulus is usually a decreasing function of J_s (i.e. an increasing function of pressure) it follows that the term p'_s is nonnegative. This means that states can exist for which p_{s1} is negative but p_s^c is positive. For such states the term $(-p_s^c\partial\hat{\phi}/\partial D_C)$ could be negative. However, the term p'_s is usually quite small (because it is essentially quadratic in elastic distortional strain) so that under most situations the coefficient of $\dot{D}_C$ will be nonnegative. Next, using the fact that $\dot{D}_C$ is nonnegative, the term ξ'_C is almost always nonnegative. This shows that the second law of thermodynamics (10) is satisfied for almost all thermomechanical processes. In practice, the value of ξ' is monitored to ensure that it remains nonnegative during all calculations.

Flow of a damaged brittle ceramic material is different from metal plasticity, which is associated with dislocation motion. Instead, the damaged brittle material flows because the comminuted material has small fragments that experience relative motion. Moreover, the effective yield strength Y (in uniaxial stress), is expected to be influenced by pore compaction and fracture growth and nucleation. Consequently, the yield strength is taken in the form

$$Y = Y_0\left\{1 - A\left[\frac{(\phi_u^0 - \phi_u^{\min})}{\phi_u^0}\right]^B\right\}I, \tag{89}$$

where Y_0 and ϕ_u^0 are the reference values of Y and ϕ_u, respectively, and A and B are material constants that are determined by matching experimental data. In the present model, plasticity is taken to be rate-independent and the deviatoric stress is limited by a yield function of the form

$$g = \frac{\sigma_e}{Y} - 1, \tag{90}$$

where σ_e is the Von Mises effective stress defined by

$$\sigma_e^2 = \tfrac{3}{2}\mathbf{T}' \cdot \mathbf{T}'. \tag{91}$$

Integration of the evolution Eq. (57a) is performed by using the method developed in Rubin and Attia (1996) which is based on the radial return procedure introduced by Wilkins (1964).

The temperature in the RVE can be determined either by integrating the balance of entropy (1) to determine a value for η, or by integrating the balance of energy (8) to determine a value for ε. For shock-wave calculations, the process is assumed to be adiabatic ($r = 0$ and $\mathbf{q} = 0$) so that it is easiest to integrate the balance of energy (8). Specifically, using the conservation of mass ($\rho J = \rho_0$) and assuming that ε vanishes in the initial state, it follows that

$$\rho_0\varepsilon = \int J(\mathbf{T}\cdot\mathbf{D})\,\mathrm{d}t. \tag{92}$$

Once the values of (J, ϕ, α_1, D_C) have been obtained by integration, the value of temperature is determined so as to satisfy the constitutive Eq. (87). For example, Eq. (87) can be rewritten in the form

$$\theta = \theta_0 + \left\{\rho_0\varepsilon + Jp_s^C\frac{\partial\phi}{\partial\theta}\theta - \frac{(1-\Phi)}{2(1+D_C)}\left[\hat{\mu}_s - \frac{\partial\hat{\mu}_s}{\partial\theta}\theta\right](\alpha_1 - 3) - (1-\Phi)(\theta_0 f_1 + f_2)\right\}\frac{1}{\rho_0 C_v}. \tag{93}$$

In general, since the temperature θ appears on the right-hand side of (93), it is necessary to solve this equation by iteration. However, for the shock-wave calculations considered here, the time step is small enough that the temperature at the end of the time step (i.e. the left-hand side of Eq. (93)) can be approximated by evaluating the right-hand side of (93) using the value of the temperature in the previous time step.

7. Examples

The objective of this section is to demonstrate physical features of the constitutive model proposed in this paper and to investigate the sensitivity of material parameters, calibrated to simulate the response of the brittle material in the examples. The first two examples consider homogeneous deformations associated with two representative loading histories. The last example considers a simulation of the inhomogeneous dynamic response in a plate-impact experiment, where a copper plate impacts a ceramic target. For this last

Table 1
Material parameters for AD-85 alumina

Constant	Equation	Value	Constant	Equation	Value
ρ_{s0} (Mg/m^3)	(41c)	3.8	C_v (J/Kg/K)	(56b)	9.21E−6
C_0 (m/s)	(70)	6630.0	θ_0 (K)	(56b)	300
S_1	(70)	0.88	γ_0	(69)	0.76
S_2	(70)	1.0	K_{IC} (GPa$\sqrt{m}$)	(13)	3.0E−6
S_3	(70)	12.0	Φ	(40b)	0.1
μ_0 (GPa)	(13)	98	ρ_0 (Mg/m^3)	(41c)	3.42
ν	(13)	0.256			

Table 2
Model parameters for AD-85 alumina (porosity)

Constant	Equation	Value
b_0'	(49c)	0.032
C_1	(55)	1.5
C_2	(55)	3.2
C_3	(52b)	7.0
p_{crush} (GPa)	(51a)	2.8
p_d (GPa)	(52a)	0.2

Table 3
Model parameters for AD-85 alumina (fracture)

Constant	Equation	Value
f_C	(15b)	0.7
κ_1	(19a)	0.3
κ_2	(19a)	0.04
κ_3 (m^{-1})	(20)	10
κ_4 (m^{-1})	(21)	3.0E+7
κ_5	(21)	1.2
τ_s (GPa)	(37c)	0.1

Table 4
Initial values ($t = 0$) for the history-dependent parameters for AD-85 alumina

Constant	Value
$\bar{a}_0$ (m)	3.0E−6
D_C	0.0
n_0 (m^{-3})	1.0E10
ϕ_u^0	0.1
ϕ_u^{min}	0.1

example, a one-dimensional shock-wave code was modified to incorporate the proposed constitutive equations, and the simulated results are compared with experimental data. The values of the material and model parameters of the ceramic are summarized in Tables 1–3, and the initial values of the history-dependent parameters are presented in Table 4. The material and model parameters remain the same for all of these examples, except for the simulations in Figs. 10 and 11, where the sensitivity of changes in a single parameter are explored.

In the following simulations, the expressions (13), (15a,b) and (19b) are calculated using a constant value for Poisson's ratio v. Also, for simplicity, the shear modulus of the solid is taken to be independent of the pressure and the temperature, so that $\mu_s(J_s, \theta) = \mu_0$ and yielding is omitted.

7.1. Homogeneous deformations

The first two examples consider homogeneous uniaxial strain deformations. For these deformations, let $\mathbf{X}$ and $\mathbf{x}$ be referred to the fixed rectangular Cartesian base vectors $\mathbf{e}_i$, and take the velocity gradient $\mathbf{L}$, the axial Lagrangian strain E_{33}, and the dilatation J in the forms

$$\begin{aligned} &x_1 = X_1, \quad x_2 = X_2, \quad x_3 = \exp(D_u t) X_3, \\ &\mathbf{L} = D_u(\mathbf{e}_3 \otimes \mathbf{e}_3), \quad E_{33} = \tfrac{1}{2}[\exp(2D_u t) - 1], \quad J = \exp(D_u t), \end{aligned} \tag{94}$$

where the symbol $\otimes$ denotes the tensor product and D_u is the constant rate of expansion/compression in the $\mathbf{e}_3$ direction, which in the following examples is taken to be $D_u = \pm 3000\ s^{-1}$.

In the first example (Figs. 1–5, a), the material is compressed until the pressure in the RVE reaches 15 GPa. Then, the sign of the deformation rate is reversed and the RVE is expanded until the dilatation reaches $J = 1.2$. At this point, the deformation rate sign is reversed again and the RVE is recompressed until gaps between the solid parts are closed. When the porosity vanishes in the RVE, compression continues until the pressure again reaches the value of 15 GPa.

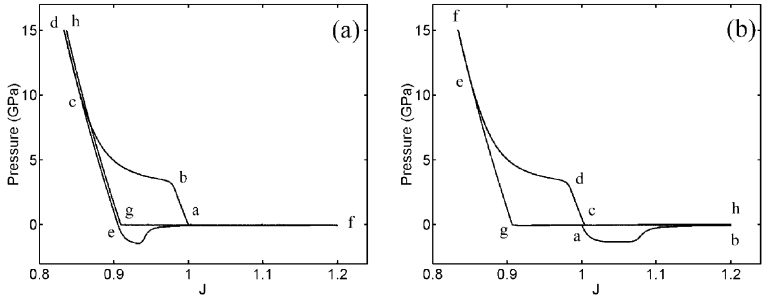

Fig. 1. Pressure in the RVE: (a) compression first, (b) expansion first.

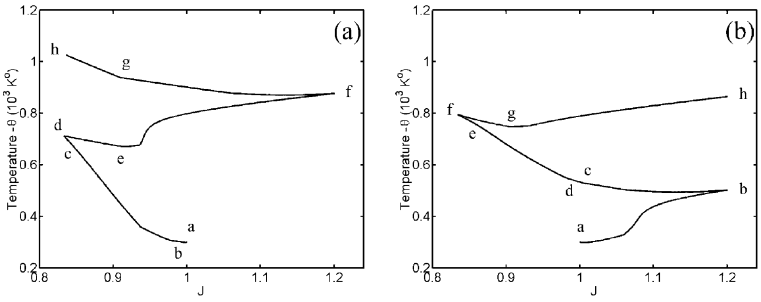

Fig. 2. Temperature in the RVE: (a) compression first, (b) expansion first.

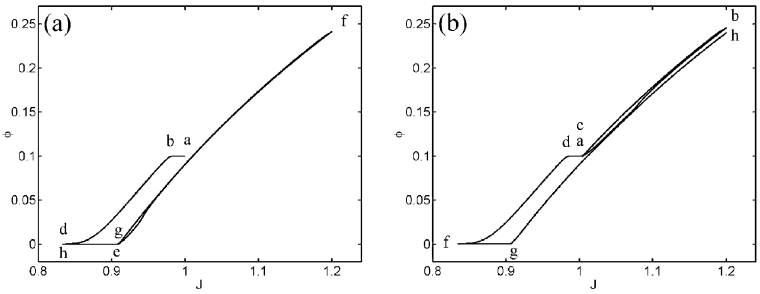

Fig. 3. Porosity in the RVE: (a) compression first, (b) expansion first.

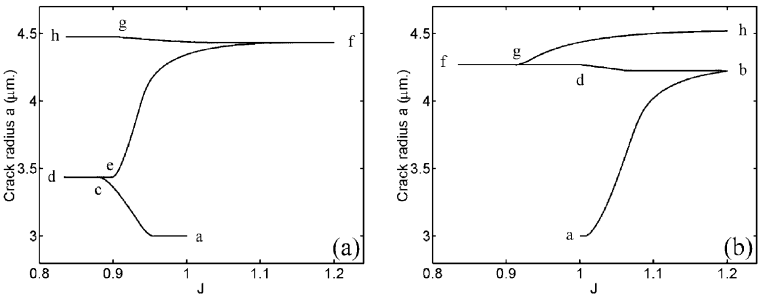

Fig. 4. Average crack radius in the RVE: (a) compression first, (b) expansion first.

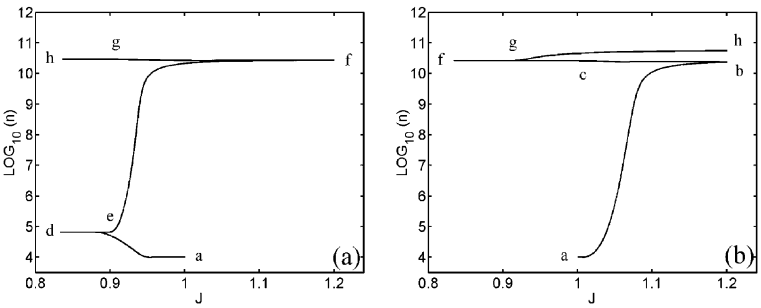

Fig. 5. Number of cracks in the RVE: (a) compression first, (b) expansion first.

In the second example (Figs. 1–5, b), loading starts with expansion until the dilatation reaches $J = 1.2$. At this point, the deformation rate sign is reversed and the RVE is compressed until gaps between the solid parts are closed. When the porosity vanishes in the RVE, compression continues until the pressure reaches the value of 15 GPa. Then, the deformation rate sign is again reversed and the RVE is expanded until the dilatation reaches $J = 1.2$.

The pressure response during these examples is shown in Fig. 1. Loading starts at point **a**, and the reader can follow the changes in the pressure during all the sequential stages. In the first example (Fig. 1a), the material behaves elastically until the pressure rises to p_{crush}, which is point **b**. Between points **a** and **b**, there is no change in the unloaded porosity ($\dot{\phi}_{\text{u}} = 0$). Above p_{crush} the pressure causes crushing of pores and the porosity decreases. When point **c** is reached, all pores are crushed and the porosity vanishes. The pressure continues to rise along the Hugoniot pressure curve up to 15 GPa at point **d**.

At point **d**, the sign of the deformation rate is reversed and the material is expanded. During unloading there is no change in the unloaded porosity ($\dot{\phi}_{\text{u}} = 0$) until the pressure becomes less than the threshold pressure ($-p_{\text{d}}$). After reaching a tensile pressure of about 2 GPa, the magnitude of the pressure in the tensile phase decreases very rapidly and the material continues to dilate with negligible resistance until point **f** is reached.

The pressure remains near zero during re-compaction, while gaps between fragments of the solid are closed with negligible resistance. After point **g** is reached ($\phi_{\text{u}} = \phi_{\text{u}}^{\min}$), the pressure increases along the Hugoniot curve. Note that the pressure curve from **g** to **h** (in Fig. 1a) does not quite follow the unloading curve from **d** to **e** because of the increase in the temperature of the material (Fig. 2a).

The temperature behavior during the two examples is shown in Fig. 2. Loading starts at point **a** where $\theta = \theta_0 = 300^{\circ}(\text{K})$ and rises according to Eq. (93). Fig. 3 exhibits the porosity ϕ and the response shown in this figure indicates that the porosity ϕ decreases with increased pressure. Figs. 4 and 5 exhibit the growth of the crack radius and the number of cracks, respectively. The response shown in these figures indicates that most of the growth occurs during the tensile phases.

The crack damage, shown in Fig. 6, is calculated by integrating the evolution Eq. (29). Thus, its value is composed of the values of the crack radius and the number of cracks in the RVE. Note that fracture related variables can only grow, as is shown in the previous three figures.

Fig. 7 shows the material integrity I. Note that the integrity in the present model is a function that characterizes modulus degradation, being the ratio of the value of the instantaneous modulus in the present configuration relative to the value of the nonporous solid modulus in the reference configuration (23). Thus, at point **a**, the integrity in both examples is less than unity due to the initial porosity. From point **a**, the integrity curves differ, depending on the loading procedure in each example. In Fig. 7a, the material undergoes compaction and the material integrity is enhanced until point **c** is reached, while in Fig. 7b the material is being dilated and its integrity degrades fast.

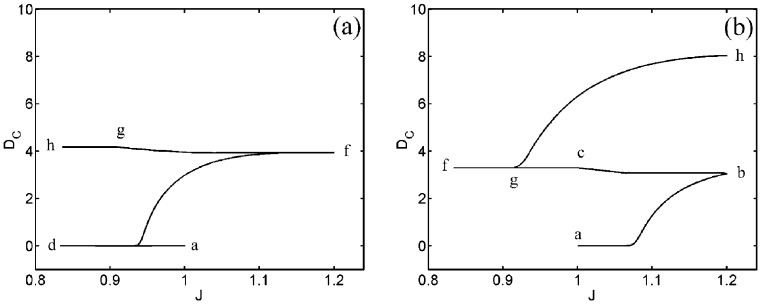

Fig. 6. Crack damage in the RVE: (a) compression first, (b) expansion first.

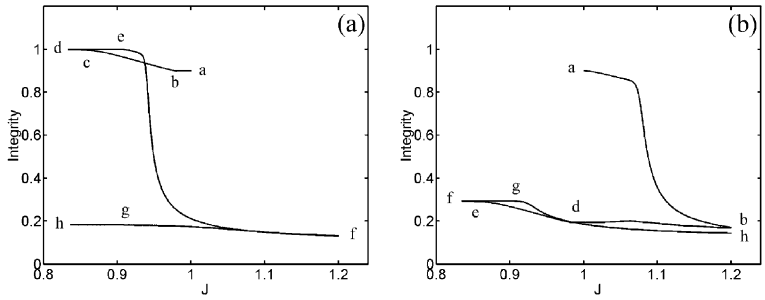

Fig. 7. Integrity of the RVE material: (a) compression first, (b) expansion first.

With regard to the pressure response in Fig. 1, it should be noted that the tensile phase (**e**–**f**) in Fig. 1a appears to be more brittle (with a more rapid reduction in tensile pressure) than the tensile phase (**a**–**b**) in Fig. 1b. The reason for this can be seen in Fig. 7, by examining the respective tensile phases of the first and second examples. The main difference between these tensile responses is due to the fact that the integrity in the first example drops faster and to a lower value during the tensile phase (**e**–**f**) than the integrity in the second example (**a**–**b**).

7.2. AD-85 plate-impact experiment

The third example is of a planar-impact experiment, which was conducted at the University of Dayton Research Institute (UDRI), and was used to demonstrate the RDG model (Rajendran et al., 1989, 1990; Rajendran and Grove, 1992). In this experiment, a 2.5 mm thick copper flyer plate impacted an 8.8 mm thick AD-85 target plate at a velocity of 570 m/s. The longitudinal stress was measured by a Manganin stress-gauge at the interface between the target plate and the PMMA back-up plate. The material data for the copper and the PMMA, which was used in the following simulation, are given in Table 5.

The material sample in the simulated plate-impact experiment was an AD-85 ceramic manufactured by Coors (Holmquist et al., 1999). Shock-wave parameters were determined by matching Hugoniot measured data from Gust and Royce (1971) and from Rosenberg and Yeshurun (1985) (see Fig. 8), and the values are presented in Table 1. The thirteen model parameters, six related to porosity (Table 2) and seven to fracture (Table 3) were calibrated to produce the best agreement with the measured axial stress (Fig. 9). Also, the initial values of the history-dependent variables are summarized in Table 4. Fig. 9 shows that the calculated axial stress almost coincides with the measured stress. It should be noted that in this example the stresses are too low for the material to exhibit any yielding. Therefore, the material in the simulation was taken to be elastic, so it was impossible to calibrate the initial yield stress Y_0 and the two parameters A, B in Eq. (89).

Stress and particle velocity histories of shock waves in ceramic materials typically exhibit ramping above the HEL (Hugoniot Elastic Limit) as shown in Fig. 9. Experimental evidence of this ramping phenomenon can be found in the work of Gust and Royce (1971), and additional evidence for the effect of porosity on the HEL stress has been given by Rosenberg (1991) and Longy and Cagnoux (1989). More recently, Bar-on et al. (2001, 2002) have shown that even though the pore volume of high-grade ceramics is quite small, it is

Table 5
Material parameters for copper and PMMA

Material	ρ_0 (Mg/m^3)	C_0 (m/s)	S_1	μ_0 (GPa)	Y_0 (GPa)
Copper	8.939	3920	2.0	455	3.0
PMMA	1.185	3070	1.295	23.2	0.25

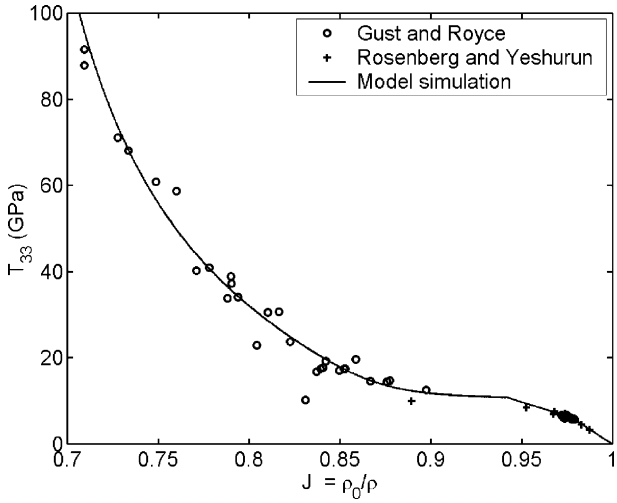

Fig. 8. Calibration of AD-85's shock-parameters using Hugoniot measurements.

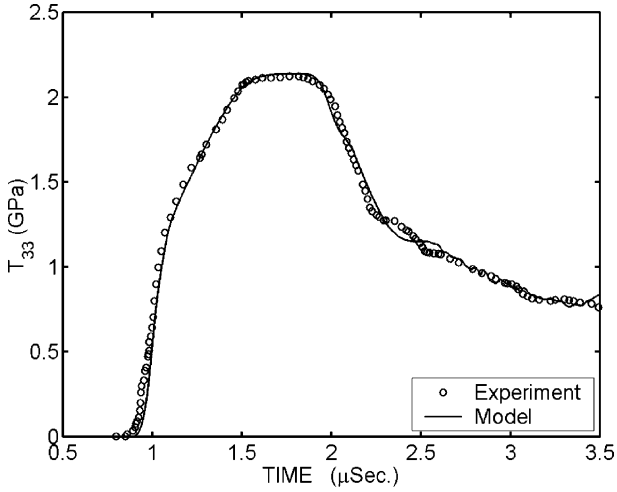

Fig. 9. Comparison of data from a plate-impact experiment with results predicted by the model.

sufficient to cause this ramping. Consequently, within the context of the present model, this ramping is characterized by the micro-mechanical mechanism of porous compaction.

7.3. Sensitivities of the material and model parameters

The values of the model parameters (Tables 3 and 4) used to simulate the experimental data (Fig. 9) were determined by trial and error. Specifically, a number of preliminary simulations were performed to determine the influence of these parameters on the wave profile. Figs. 10 and 11 exhibit the influence of the model parameters associated with porosity (Table 2) and fracture (Table 3), respectively, as well as the influence of the initial values ϕ_u^0 of ϕ_u and n_0 of n. For each of the simulations in these figures only one

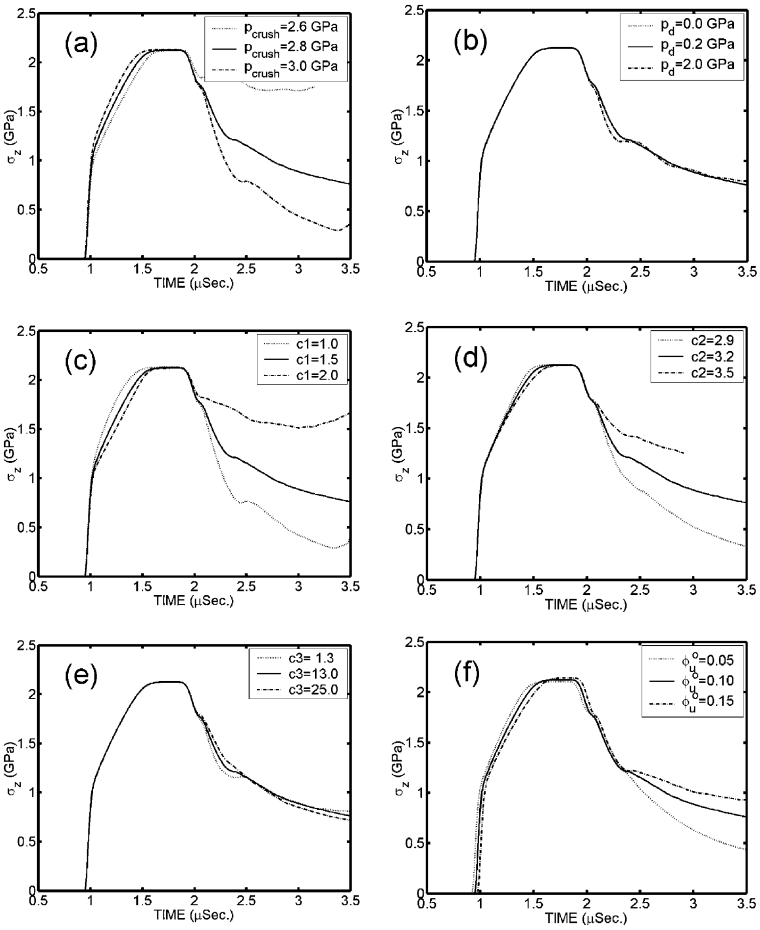

Fig. 10. Influence of the model parameters associated with porosity.

model parameter was varied, with the remaining parameters being specified by the values given in Table 1–3. Also, the solid lines in these curves use the value of the specific material parameter given in these tables which best simulate the experimental data, as shown in Fig. 9.

From Fig. 10a it can be seen that threshold pressure p_{crush} controls the stress level at which porous compaction begins. This parameter influences the ramping portion of the loading phase above the HEL as well as the fracture portion of the release phase. Fig. 10b shows that the material response in this high pressure shock-wave experiment is relatively insensitive to changes in the parameter p_{d}, which controls the spall strength. Consequently, for high pressure shock waves in ceramics, it can be assumed that porosity starts to grow as soon as the pressure becomes negative (tension), and that $p_{\text{d}} = 0$. However, for the low pressure response of ceramics the failure in tension will be more sensitive to the value of p_{d} so that a nonzero value of p_{d} can be determined from the experimental data.

Fig. 10c and d explore the effects of the model parameters C_1 and C_2, which control porous compaction and which appear in the function $f_3(p, p_{\text{crush}})$ in (51) and in (55). From these figures it can be seen that these parameters influence both the loading and release phases of the wave profile. Fig. 10e shows that wave profile is relatively insensitive to changes in the parameter C_3, which controls porous dilation in (52a).

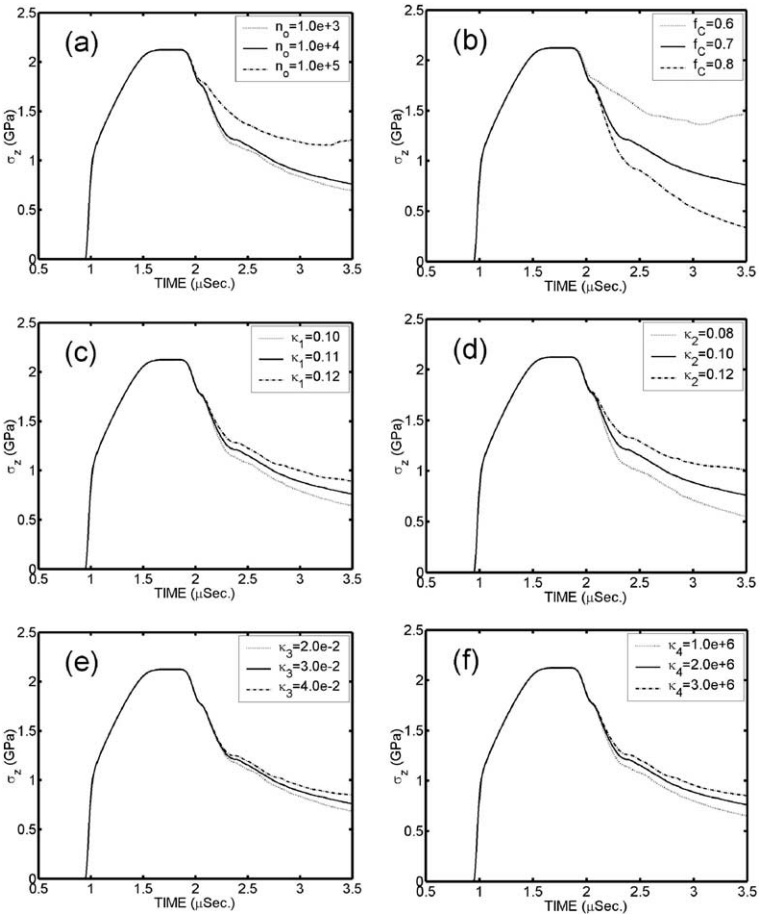

Fig. 11. Influence of the model parameters associated with fracture.

The initial value ϕ_u^0 of the unloaded porosity ϕ_u is determined by the reference value ρ_0 of the mass density of the porous material and the theoretical reference value ρ_{s0} of the solid matrix material. However, it is still of interest to explore the influence of this parameter on the wave profile. Fig. 10f shows that changes in ϕ_u^0 influence the arrival time of the wave as well as the lower portion of the release phase.

Next, attention is turned to the model parameters discussed in Section 3 which control fracture. Note from Fig. 11 that these parameters effect only the release phase of the wave profile. Specifically, it is recalled that that the number of cracks n per unit volume in the RVE appears in the crack distribution function (Eq. (11a)) and in the evolution Eq. (20) for crack nucleation due to the "branching" phenomenon. Fig. 11a shows that when the initial number of cracks in the material (n_0) is increased, the damage developed during the release phase of the experiment is also increased. This damage is responsible for loss of material integrity which causes the curve that describes the stress transmitted to the PMMA to decrease with a milder slope.

The coefficient of friction f_C effects damage growth and nucleation when the normal stress acting on a crack surface is compressive. Even though this parameter is specified to be a constant in this work, it probably depends on other state variables, like pressure and maybe also on the percentage of the crushed pores. Fig. 11b shows that this parameter significantly effects the magnitude of damage. More specifically,

damage occurs when the release wave, reflected from the rear face of the projectile, causes the material to lose integrity due to fracture under tensile stress. The common values found in the literature are around 0.7 (see Rajendran and Grove, 1992).

The next four material parameters considered, influence the rate equations characterizing fracture mechanics. Specifically, the parameters κ_1 and κ_2 in Eq. (19a) control the rate of increase of the average crack length $\bar{a}$. The first parameter κ_1 multiplies the expression for crack growth-rate and the second parameter κ_2 is the exponent of the ratio between the critical energy release rate and the instantaneous energy release rate. The effects of varying these material parameters are shown in Fig. 11c and d, respectively.

The parameter κ_3 in Eq. (20) multiplies the expression for the rate of crack nucleation due to branching, and the parameter κ_4 in Eq. (21) multiplies the expression for crack nucleation rate due to the generation of cracks while pores are crushed in compression. The effects of varying these material parameters are shown in Fig. 11e and f, respectively. From these figures it can be seen that these material parameters effect the material response by degrading the strength of the material as the release wave moves through the ceramic plate. An increase in damage causes weakening of the ceramic which leads to a milder slope in the release phase of the wave profile.

In general, it can be seen from Figs. 10 and 11 that the influences of most of the model parameters on the wave profile are not uncoupled. This means that it is not possible to determine unique values for these parameters without considering a series of different experiments. However, since the model parameters for fracture effect only the release phase of the wave profile it is possible to first adjust the model parameters for porosity to match the loading phase and then to adjust the model parameters for fracture to match the release phase. This procedure leads to the excellent comparison between experiment and simulation shown in Fig. 9.

In order to model the influence of load history on the crack propagation speed, and to enhance the capability of the present model to simulate experiments with various boundary conditions, it may be necessary to specify functional forms for the values of κ_1, κ_2, κ_3 and κ_4 which depend on state variables. In particular, the values of these parameters may be different for states of tension and compression. However, for the plate-impact experiment simulated in this work, it was sufficient to choose these parameters to be constants.

8. Summary

The present work uses fracture mechanics criteria for penny-shaped cracks and phenomenological equations for pores to develop a macroscopic constitutive model for simulating the response of brittle materials. A functional form for the Helmholtz free energy is proposed and constitutive equations are determined by satisfying the first law of thermodynamics. The examples indicate that the theoretical predictions of the model are in excellent agreement with experimental data from a plate-impact test.

References

Achenbach, J.D., 1973. Wave Propagation in Solids. North-Holland Publishing Co.

Bar-on, E., Yankelevsky, D.Z., 1993. Using Maxwell–Boltzmann's statistics for microcracks distribution function in a failure model. In: Proceedings of the APS Shock Waves in Condensed Matter Conference. Colorado-Springs, Co, pp. 1165–1168.

Bar-on, E., Partom, Y., Rubin, M.B., Yankelevsky, D.Z., 2001. On the HEL and the ramping above HEL. In: Proceedings of the APS Shock Waves in Condensed Matter Conference. Atlanta, GA, pp. 739–742.

Bar-on, E., Partom, Y., Rubin, M.B., Yankelevsky, D.Z., 2002. Porous compaction as the mechanism causing the Hugoniot elastic limit. Int. J. Impact Eng. 37, 509–520.

Budiansky, B., O'Connell, R.J., 1976. Elastic moduli of cracked solid. Int. J. Sol. Struct. 27, 81–97.

Green, A.E., Naghdi, P.M., 1977. On thermodynamics and the nature of the second law. Proc. R. Soc. London A357, 253–270.
Green, A.E., Naghdi, P.M., 1978. The second law of thermodynamics and cyclic processes. ASME J. Appl. Mech. 45, 487–492.
Griffith, A.A., 1924. Theory of rupture. In: Proceedings of the First Int. Cong. for Applied Mechanics, pp. 55–63.
Gust, W.H., Royce, E.B., 1971. Dynamic yield strength of B_4C, B_eO and Al_2O_3 ceramics. J. Appl. Phys. 42 (1), 276–295.
Hashin, Z., 1964. Theory of mechanical behaviour of heterogeneous media. Appl. Mech. Rev. 17, 1–9.
Hashin, Z., 1983. Analysis of composite materials—a survey. J. Appl. Mech. 50, 481–505.
Hill, R., 1963. Elastic properties of reinforced solids: some theoretical principles. J. Mech. Phys. Solids 11, 357–372.
Holmquist, T.J., Rajendran, A.M., Templeton, D.W., Bishnoi, K.D., 1999. A ceramic Armor material database. TARDEC Technical Report.
Horii, H., Nemat-Nasser, S., 1983. Overall moduli of solids with micro-cracks: load-induced anisotropy. J. Mech. Phys. Solids 31, 155–171.
Ju, J.W., 1990. Isotropic and anisotropic damage variables in continuum damage mechanics. J. Eng. Mech. Div. ASCE 116, 2764–2770.
Kachanov, L., 1958. On the time to rupture under creep conditions. Izv. Acad. Nauk SSSR, OTN 8, 26–31.
Kachanov, M., 1992. Effective elastic properties of cracked solids: critical review of some basic concepts. Appl. Mech. Rev. 45 (8), 304–335.
Kachanov, M., 1993. On the effective moduli of solids with cavities and cracks. Int. J. Fract. 59, R17–R21.
Kachanov, M., 1994. On the concept of damage in creep and in the brittle-elastic range. Int. J. Damage Mech. 3, 329–337.
Kachanov, M., Tsurkov, I., Shafiro, B., 1994. Effective moduli of solids with cavities of various shapes. Appl. Mech. Rev. 47 (1), S151–S174.
Keer, L.M., 1966. A note on shear and combined loading for a penny-shaped crack. J. Mech. Phys. Solids 14, 1–6.
Krajcinovic, D., 1996. Damage Mechanics. In: North-Holland Series in Applied Mathematics and Mechanics, vol. 51. Elsevier, Amsterdam, The Netherlands.
Kröner, E., 1977. Bounds for effective elastic moduli of disordered materials. J. Mech. Phys. Solids 25, 137–155.
Longy, F., Cagnoux, J., 1989. Plasticity and microcracking in shock-loaded alumina. J. Am. Ceram. Soc. 72, 971–979.
Margolin, L.G., 1983. Elastic moduli of a cracked body. Int. J. Fract. 22, 65–79.
Nemat-Nasser, S., 1986. Overall stresses and strains in solids with microstructure. In: Gittus, J., Zarka, J. (Eds.), Modeling Small Deformations of Polycrystals. Elsevier Publishers, Netherlands, pp. 41–64.
Nemat-Nasser, S., Hori, M., 1993. Micromechanics: Overall Properties of Heterogeneous Materials. In: Achenbach, J.D., Budiansky, B., Lauwerier, H.A., Saffman, P.G., Van Wijngaarden, L., Willis, J.R. (Eds.), North-Holland Series in Applied Mathematics and Mechanics, vol. 37.
Rajendran, A.M., Grove, D.J., 1992. Modeling the impact behavior of AD-85 ceramic. In: 24th Int. SAMPE Technical Conf. T925-T934.
Rajendran, A.M., Dietenberger, A.M., Grove, D.J., 1989. A void-based failure model to describe spallation. J. Appl. Phys. 65 (4), 1521–1527.
Rajendran, A.M., Dietenberger, A.M., Grove, D.J., Cook, W.H., 1990. A dynamic failure model for ductile materials. UDR-TR-90-109.
Rice, J.R., 1984. Comments on "On the stability of shear cracks and the calculation of compressive strength" by J.K. Dienes. J. Geophys. Res. 89 (B4), 2505.
Rosenberg, Z., 1991. The response of ceramic materials to shock loading. In: Proceedings of the APS Shock Waves in Condensed Matter Conference, Williamsburg, VA, 1991.
Rosenberg, Z., Yeshurun, Y., 1985. Determination of dynamic response of AD-85 alumina with in-material manganin gauges. J. Appl. Phys. 58 (8), 3077–3080.
Rubin, M.B., 1986. An elastic-viscoplastic model for large deformation. Int. J. Eng. Sci. 24 (7), 1083–1095.
Rubin, M.B., 1992. Hyperbolic heat conduction and the second law. Int. J. Eng. Sci. 30, 1665–1676.
Rubin, M.B., Attia, A.V., 1996. Calculation of hyperelastic response of finitely deformed elastic-viscoplastic materials. Int. J. Numer. Meth. Eng. 39, 309–320.
Rubin, M.B., Elata, D., Attia, A.V., 1996. Modeling added compressibility of porosity and the thermomechanical response of wet porous rock with application to MT. Helen Tuff. Int. J. Solids Struct. 33 (6), 761–793.
Rubin, M.B., Vorobiev, O.Y., Glenn, L.A., 2000. Mechanical and numerical modeling of a porous elastic-viscoplastic material with tensile failure. Int. J. Solids Struct. 37, 1841–1871.
Segedin, M.C., 1950. Note on a penny-shaped crack under shear. Proc. Cambridge Philos. Soc 47, 396–399.
Sneddon, N.I., 1969. The distribution of stress in the neighbourhood of a crack in an elastic solid. In: Crack Problems in the Classical Theory of Elasticity. Wiley, New York.
Steinberg, D.J., 1991. Equation of state and strength properties of selected materials. UCRL-MA-106439.
Wilkins, M.L., 1964. Calculation of elastic–plastic flow. In: Methods in Computational Physics, vol. 3. Academic Press, New York, pp. 211–263.
Willis, J.R., 1981. Variational and related methods for the overall properties of composites. Adv. Appl. Mech. 21, 1–78.